Extracting Oil Slick Features From VIIRS Nighttime Imagery Using a Gaussian Filter and Morphological Constraints

Mengqiu Wang and Chuanmin Hu

***Abstract*—Satellite images of reflected sunlight have been used to detect and monitor oil spills in oceans. However, such a capacity is often hindered by the image noise due to either a low signal-to-noise ratio or other image features such as clouds or cloud shadows. The problem is particularly severe for nighttime images captured by the Visible Infrared Imager Radiometer Suite (VIIRS). This letter proposes a practical method to extract oil slick features in a semiautomatic fashion from VIIRS nighttime images and other noisy optical remote sensing images. The method is based on statistical information and morphological operators, and it is demonstrated to be able to effectively remove the noise and identify line features with the appropriate selection of threshold values. Testing this method over VIIRS nighttime images shows the preliminary success of oil slick feature extraction. Experiments on daytime data collected by the Moderate Resolution Imaging Spectroradiometer (MODIS) also suggest the applicability of this method to other optical remote sensing images. However, the requirement of human intervention to determine optimal parameters points to the need for improved automation in future works.**

***Index Terms*—Day–night band (DNB), feature extraction, moderate resolution imaging spectroradiometer (MODIS), moon glint, morphological operator, noise reduction, oil slicks, visible infrared imager radiometer suite (VIIRS).**

I. Introduction

OIL spills can cause serious damage to marine and coastal ecosystems [1]. According to a U.S. National Academy of Sciences report in 2003 [2], natural oil seeps account for a large percentage of crude oil entering the ecosystem; hence, ecological adaptations can occur at a geological time scale. Remote sensing techniques, with the development of state-of-the-art sensors and algorithms, serve as effective means to monitor and assess oil pollution in oceans and to guide coastal resource management [3]–[5].

Currently, most satellite observations of oil spills in oceans rely on synthetic aperture radar (SAR) data [6] because of their high spatial resolution, transparency to most clouds, and day–night operability. On the other hand, Hu *et al.* [7], Chust and Sagarminaga [8], and others have demonstrated that optical sensors such as MODIS also have the capacity to detect oil spills under sun glint based on the similar wave-damping principles as used by SAR. The Visible Infrared Imager Radiometer Suite (VIIRS) has similar orbital characteristics and a wider swath than MODIS [9] and thus is also suitable for oil spill detection under sun glint and cloud-free conditions. Indeed, VIIRS imagery collected at night may be also used to capture oil slick features under moon glint [10].

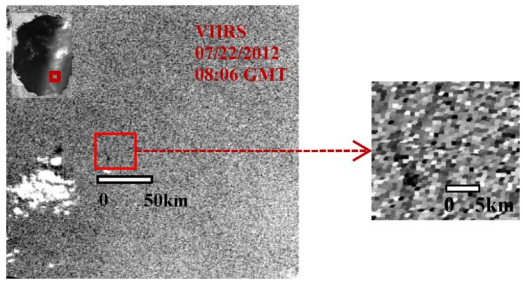

Fig. 1. Pixelization noise on VIIRS nighttime imagery over the GOM (inset image) under moon glint, with a small portion in the SW GOM extracted to show the noise over which a slick-like feature may be visible.

A major obstacle in the routine application of oil slick feature extraction from optical remote sensing imagery is image noise and other natural features. This is particularly true for VIIRS nighttime imagery where image pixelization noise is apparent (see Fig. 1) due to its low SNR. Most detectable slick features are only 2–3 pixels wide for medium-resolution sensors (e.g., 375–750 m for VIIRS and 250 m for MODIS); this presents the technical challenge of preserving the small features while suppressing noise. An efficient algorithm to reduce noise contamination is required to extract the oil slick features, particularly from low-SNR imagery.

On SAR images where the noise strongly influences the feature extraction results, geometric filters and edge detection algorithms are often used to extract oil slick features. Although nonparametric spatial smoothing filters such as enhanced Frost, enhanced Lee, Gamma, and Kuan filters can use large convolution templates to get satisfactory results (i.e., smoothed features), they also simultaneously blur the shape boundary and decrease the accuracy of feature extraction [11], [12]. Edge detection algorithms face a similar issue, where a small convolution window preserves noise, whereas a larger window blurs slick features [12]. Parametric filters such as a Gamma–Gamma maximum *a posteriori* filter and a Weibull multiplicative model

Manuscript received November 10, 2014; revised March 11, 2015 and June 1, 2015; accepted June 8, 2015. Date of publication July 2, 2015; date of current version August 7, 2015. This work was supported in part by the National Aeronautics and Space Administration through the Ocean Biology and Biogeochemistry Program, by the U.S. Bureau of Ocean Energy Management, by the Center for Integrated Modeling and Analysis of Gulf Ecosystems (C-IMAGE), by the National Oceanic and Atmospheric Administration's National Environmental Satellite, Data, and Information Service, by the Anne and Werner Von Rosenstiel Endowed Fellowship, by the Gulf Oceanographic Charitable Trust Endowed Fellowship, and by the William and Elsie Knight Endowed Fellowship.

The authors are with the College of Marine Science, University of South Florida, St. Petersburg, FL 33701 USA (e-mail: mengqiu@mail.usf.edu; huc@usf.edu).

Color versions of one or more of the figures in this paper are available online at http://ieeexplore.ieee.org.

Digital Object Identifier 10.1109/LGRS.2015.2444871

(WMM) filter assume a predefined noise distribution, and they can result in satisfactory results when appropriate parameters are selected [13], [14]. However, in our case, even after the parameters were optimized, the WMM filter did not lead to better results than a Gaussian filter (see comparisons in the supplemental materials).[1] This might be due to the imperfect assumption in modeling noise distributions. An improved thresholding method is also adopted in the dark-spot detection process on SAR imagery for its simplicity [15]. Although other approaches used for boundary detection and image segmentation in SAR images such as the level set method, the active contour model [12], and the minimum description length principle [16] have yielded better results than intensity thresholding methods, they require a higher SNR and are more computationally expensive. Both the geometry information and the contextual features are commonly used in oil slick extraction in SAR imagery [4], [17]. Texture-based classification schemes (e.g., see [18]) require ancillary information such as wind to rule out other look-alikes. Some preprocessing methods such as anisotropic diffusion filtering and morphological leveling [19] have been proposed to facilitate feature extraction.

In short, nearly all feature extraction methods were designed for SAR imagery. It is still not clear to our knowledge how to best extract slick features from noisy optical imagery from MODIS or VIIRS that also contain pixelization noise and other features such as clouds, cloud reflection, cloud shadows, striping, etc. Thus, the primary objective of this letter is to develop a practical method to extract oil slick features from noisy VIIRS nighttime images. The second objective is to test the general applicability of the method to other types of optical images (e.g., MODIS). In the following section, the method is described in detail, followed by examples to demonstrate its effectiveness and discussions on its limitations.

II. Method

In contrast to earlier satellite instruments such as the Operational Linescan System, the VIIRS day–night band (DNB) is well calibrated [20], yet its nighttime detection ability is still limited by the moonlight illumination geometry [21]. For oil spill detection, moon glint is required to increase the SNR and to increase the contrast between oil slick features and the background. Despite that, the SNR often ranged between 30:1 and 50:1 [10], and differentiating oil slick features requires specialized knowledge by trained researchers.

Because oil slick features often have relatively narrow widths (one to several pixels) particularly when they come from natural seeps, noise filtering should both preserve the narrow features and avoid breaking coherent line features. A Gaussian filtering window can be applied to achieve this. Slick features inevitably become exaggerated after spatial smoothing. Thus, a threshold filter and low-intensity (referring to a relatively small smoothing window) spatial smoothing are applied to allow the discovery of slick-like features. Comparisons of the Gaussian filter with other popular approaches such as a diffusion anisotropic filter, the Weibull filter [23], etc., are presented and discussed in the supplemental materials.

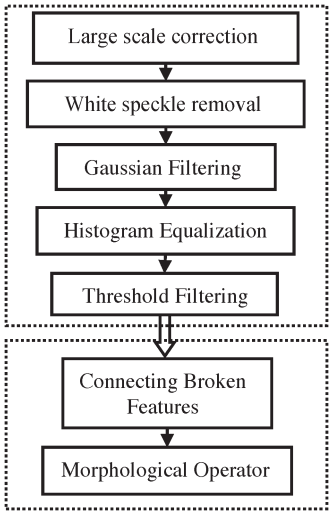

Fig. 2. Workflow of the feature extraction method. The individual steps are grouped into two processes, which are outlined by the dotted rectangles.

Oil slicks can appear brighter (positive) or darker (negative) than the background, depending on the locations of the slicks relative to the glint zone [7], [22], [24]. To unify the process, for images with brighter features, an inverse procedure is used to reverse the contrast before applying the detection method. Some images contain strong spatial gradients due to nonuniform glint signals. Then, for areas of interest (AOIs) with a strong gradient across the pixels (e.g., from the glint center to the glint edge), a roaming window is used to subtract a background mean from the original pixel value in order to balance the image. Such large-scale correction is only required when strong gradients exist; thus, it is not described in the workflow.

In summary, the seven-step method can be classified into the following two processes, as shown in Fig. 2.

A. Digital Enhancement

To facilitate the feature extraction, the first task is removing salient noisy pixels. This is because the noise pixels have similar pixel values with oil slicks and thus will interfere with the feature extraction. We define obtrusive noise pixels as those bright pixels whose neighbors are all darker pixels. The threshold to delineate these noise pixels is given by

$$\text{wthr} = (\text{maxvl} - \text{minvl}) \times 0.4 \tag{1}$$

where wthr is the threshold value, and maxvl and minvl are the maximum and minimum pixel values of the AOI, respectively. The empirical number 0.4 is determined through trial and error using the standard that all the isolated bright pixels are noise due to the reflectance difference of oil and water [1]. Then, a 3×3 Gaussian filter is applied to suppress the noise and obtain coherent features [see Fig. 3(a) and (b)].

After removing the isolated noise pixels, histogram equalization, with the appropriate cut-down value, is applied to the AOI. The equalization is based on the area's statistical range after which dark slick features are more distinct from the background [see Fig. 3(c)]. The statistical range is selected based on the

[1]This paper has supplementary downloadable material available at http://ieeexplore.ieee.org, provided by the authors.

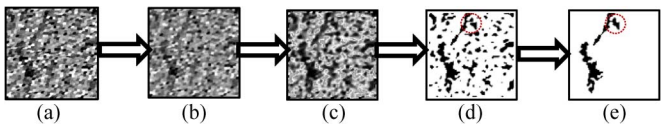

Fig. 3. Procedures in the feature extraction method. (a) Original image. (b) Gaussian filtered result. (c) After histogram equalization. (d) After threshold filtering. (e) Final features extracted after applying feature connection and the morphological constraints. Note that the red circles in (d) and (e) show the discrete slick features (d) joined after feature connection, thus preserving the final detection result (e).

AOI's histogram. Typically, $0.5 \times$ maxvl is the cutoff value for bright pixels, and minvl is the cutoff value for darker pixels.

Next, a threshold filter is used to filter all bright pixels while retaining the darker pixels. The threshold value is set as

$$\text{thr} = A \times \text{stdev} \tag{2}$$

where stdev represents the standard deviation of the AOI, and A is a scaling factor ranging from 0.2 to 0.8 for different images. Because no direct correlation between this threshold and either the mean or the stdev value of the AOI has been found, a derived scaling factor relationship cannot be applied to every image. This is typical for image segmentation. For example, Otsu's image segmentation threshold method [25], which selects the threshold that has the maximum cross-class-variance-to-in-class-variance ratio, is also unable to provide a general solution. Indeed, the Otsu threshold method works fine for MODIS images but requires adjustment for VIIRS nighttime images with a lower SNR. We have tested the sensitivity of the feature extraction performance to variable A, and we found stable performance for A around 0.4 (see supplemental materials).

The image segmentation performance of the threshold-filter-based approach in this letter was compared with other well-known segmentation methods, such as the level set method, the mean shift, the Markov random field, and fuzzy c-means methods. The results show that the level set and fuzzy c-means methods can be good substitutes for Steps 4 and 5 in our workflow. However, the smooth boundary that resulted from the level set approach is often less accurate. The fuzzy c-means method, which has been used in oil slick extraction on MODIS imagery [27], generally shows a satisfactory extraction result, but it is hard to adjust when an imperfect result occurs. Other methods yield less satisfactory performance than our proposed method when applied to VIIRS nighttime imagery (see supplemental materials).

B. Morphological Constraints

The resulting image after Step 3 [e.g., see Fig. 3(c)] still contains noise or other unwanted features primarily due to the low SNR. Furthermore, due to noise contamination or the strict threshold value used in Steps 1–3, some coherent features may break into separate parts. These "broken" features are connected through a direction search operator in the following way. Oil slicks are programmatically defined as contiguous suspect pixels. For each unmarked (i.e., nonoil) pixel, the operator searches its eight neighboring pixels. If this pixel connects two unconnected oil slicks, the operator then marks it as an oil pixel, and the two features are joined into one. Oil features separated by more than two pixels are considered discontinuous features.

After connecting the broken features, a morphological operator is introduced to determine whether the shape of the detected feature is oil. Although oil slicks can have various shapes, the oil features in our cases are more elongated than the noise patches due to ocean currents (see [7]). The geometric and shape features have been also adopted in related studies to characterize the oil slicks [4]. In a recent publication, elongated features are also used to characterize oil slicks and to identify oil seep locations in the Caribbean [26]. The degree of elongation has been also used in oil slick extraction on SAR imagery [4]. The operator works in two steps. First, the number of pixels in the feature should be larger than a predefined threshold, i.e., Min_pnum. The threshold is initially set to be 0.5% of the AOI area as a reference, which could be adjusted to gain optimal performance. The roundness is calculated as

$$R_{\text{factor}} = \frac{4\pi S}{c^2} \tag{3}$$

where S is the area of the feature, and c is the circumference. A feature's roundness value must be lower than the roundness threshold in order to be classified as oil. Fig. 3(e) shows the final result after applying the direction search operator and the morphological operator to the data shown in Fig. 3(d).

Because the semiobjective detection still requires some human intervention, a graphical user interface was developed using the Interactive Data Language to facilitate the selection of AOIs and parameter optimization.

III. Experimental Results

In this section, the experimental results derived from two VIIRS nighttime images and one MODIS daytime image are presented and discussed. The test region is the NW Gulf of Mexico (GOM) bound by 25° N to 30° N and 94° W to 90° W. This is the region where satellite imagery often captures surface oil slicks from natural oil seeps [7]. Due to the lack of ground-truthing data, the validity of the method is evaluated using two criteria: 1) do the delineated features visually correspond to features found in the raw imagery; and do the delineated features overlap with those recurrent features from known seep locations? These recurrent features were determined to be from oil seeps after ruling out other possible causes such as wind, surfactants from phytoplankton blooms, or oil released from ships [7], [28].

The first case (see Fig. 4) shows the feature extraction of negative contrasting pixels from the VIIRS nighttime data collected on January 25, 2013 at 07:00 GMT. The AOI is 50×50 pixels. The threshold for filtering the dark pixels is set as $0.61 \times$ stdev, and the roundness threshold is set as $0.1 \times \pi$. The minimum number of pixels for each slick feature is 20. The results are presented in Fig. 4(a) and (b). For comparison, after applying the same procedure with similar parameters ($0.7 \times$stdev, $0.1 \times \pi$, and 30 pixels), the results from the MODIS daytime image (80×80 pixels) on June 2, 2005 are shown in Fig. 4(c) and (d). The proximity of the derived VIIRS slick feature correlates well to the known seep locations inferred from the MODIS-derived slicks and the general slick morphology, although their exact shapes and orientations are different due to different image collection times.

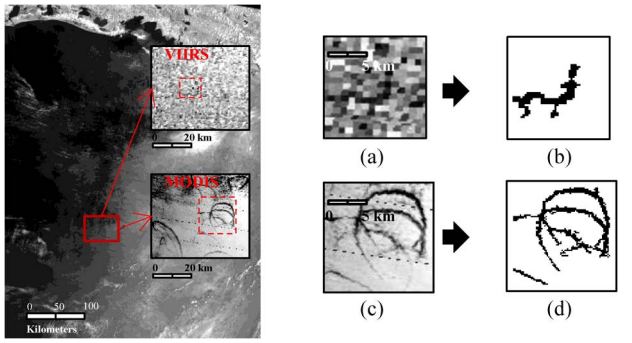

Fig. 4. Example of oil slick extraction on pixels with a negative contrast. The background image to the left shows the NW GOM. The two inset images are the VIIRS nighttime (January 25, 2013) and MODIS daytime (June 2, 2005) images at the same location. (a) and (b) VIIRS raw image and final extraction results, respectively. (c) and (d) Results for MODIS. Note that the periodic dotted lines in the MODIS image due to sensor artifacts are removed by the feature extraction procedure.

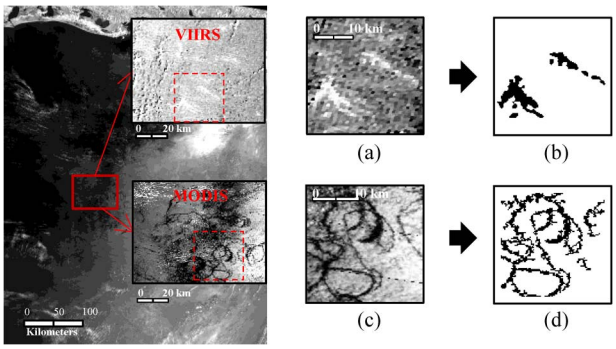

Fig. 5. Same as Fig. 4, but the VIIRS slicks show positive contrasts. The VIIRS nighttime image was collected on September 5, 2012, whereas the MODIS daytime image was collected on June 2, 2005.

The second case shows the feature extraction of positive contrasting pixels from the VIIRS nighttime data collected on September 5, 2012 at 08:07 GMT (see Fig. 5). The AOI contains 120 × 120 pixels. The three parameters are set to 0.32 × stdev, 1 × π, and 20 pixels, respectively. The results are presented in Fig. 5(a) and (b). The corresponding MODIS results (100 × 100 pixels) are shown in Fig. 5(c) and (d) after using the following parameters: 0.7 × stdev, 0.1 × π, and 30 pixels.

To test the effectiveness of the procedure over large areas, two regions in the NW GOM that exhibit negative [see Fig. 6(a)] and positive contrasting [see Fig. 6(d)] slick features, respectively, are used. In each region, several AOIs are first defined [the gray rectangles in Fig. 6(b) and (e)], with the procedure applied to each area using customized thresholds and parameters. The results from all areas are merged to compose the final images, as shown in Fig. 6(b) and (c) for the negative contrasting features and in Fig. 6(e) and (f) for the positive contrasting features. Similar to Fig. 6, Fig. 7 shows the results for the VIIRS nighttime image. Although the parameters have to be tuned for some AOIs, the tuning is minimal or none for features with a similar background. After registering these images to other coregistered MODIS images where similar slick features are identified, it is found that the slicks delineated in Figs. 6 and 7 are recurring features, thus suggesting that they are likely oil slicks from natural seeps in the GOM. Note that

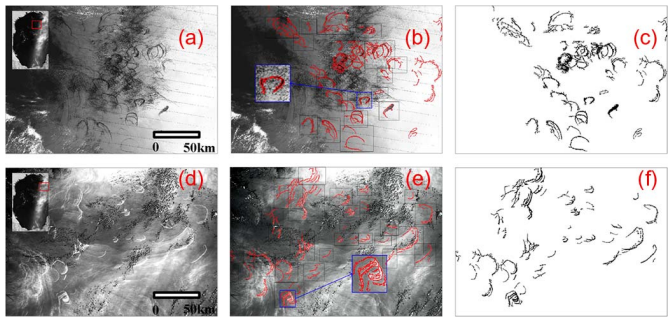

Fig. 6. Oil slick feature extraction from the MODIS daytime image on June 2, 2005. (a) and (d) Raw image in different regions of the NW GOM. (b) and (e) Outlines (in red) of the slick extraction results overlaid on the original images. (c) and (f) Extraction results. The two slicks [insets in (b) and (e)] indicated by the blue arrows are enlarged to show the details.

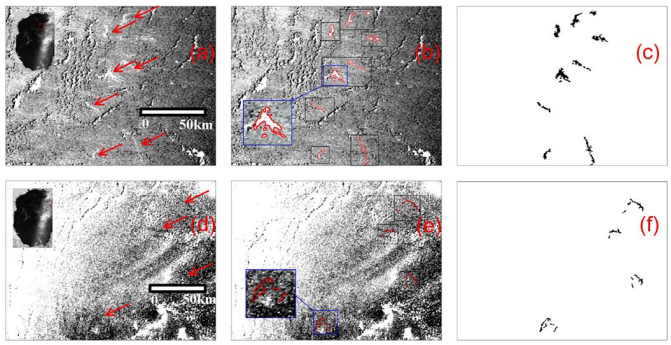

Fig. 7. Same as in Fig. 6, but the procedure is applied to the VIIRS nighttime image collected on September 5, 2012. The arrows indicate slick locations.

TABLE I
ACCURACY ASSESSMENT STATISTICS FOR THE OIL SLICK FEATURE EXTRACTION RESULTS ON THE VIIRS NIGHTTIME IMAGE SHOWN IN FIG. 7

	Min	Max	Mean	75th percentile	Standard Deviation
Commission Error	0.012	0.224	0.105	0.177	0.071
Omission Error	0.034	0.406	0.260	0.349	0.102

all image noise and artifacts such as the periodic dotted lines are removed in the final images.

Similar to the evaluation of the SAR oil slick extraction performance where the "truth" is often provided by a human expert, the accuracy of the segmentation method is quantitatively evaluated through a visual interpretation using the criteria of commission and omission errors [15], [29]. The commission error is the percentage of pixels within a certain distance of the manually selected spots that are erroneously classified as the oil of the total detected feature. The omission error is the percentage of pixels within a certain distance of the computer-detected spots that are erroneously identified as the background of the total manually selected feature. Table I lists the accuracy statistics on the VIIRS experiment shown in Fig. 7. Two subset images are compared with the human-delineated results using the Environment for Visualizing Images (ENVI) region-of-interest tools. The labeling of each pixel is through the human visual interpretation. The distance for measuring the commission and omission errors is set as one pixel. The mean omission error is 26%, with a standard deviation of 10%. The

mean commission error is 10%, with a standard deviation of 7%. The worst case has an omission error of 44%. More than 75% of the cases have omission errors < 35%. For the MODIS experiment, the extraction accuracy is higher.

IV. Discussion and Conclusion

A new feature extraction method has been developed to extract oil-like slick features from noisy VIIRS DNB imagery and MODIS imagery in a semiautomatic fashion. This is because the low SNR of the VIIRS DNB imagery and many other features in both the VIIRS and MODIS images make it extremely difficult to extract features automatically, and previously established methods for SAR image segmentation do not work well. The SNR of the VIIRS DNB imagery under moon glint used in this letter has been estimated to be 30:1–50:1 [10] based on the method of Hu *et al.* [30]. The feature extraction method is based on a series of processing steps including digital enhancement and morphologic operations in order to delineate slick features from the noisy background, which often contains other image features. The examples here show preliminary success in extracting oil slick features from the VIIRS DNB imagery. Further experiments indicate its general applicability to MODIS daytime imagery (645- and 859-nm bands) for their higher spatial resolution and higher SNRs. The method, however, requires human intervention to determine the optimal threshold values and thus cannot be fully automated at this stage. Under certain circumstances, the roundness parameters and the minimum pixel number both need to be adjusted in order to retain suspect features while removing noise [e.g., see Fig. 5(a) and (b)]. This is particularly true over large areas where there may be both positive and negative contrasting features within a single image. Future efforts therefore may be dedicated to automatically determining parameters in the segmentation process, where a roaming window can be adopted to loop through the entire image with reduced human interaction. In any case, given the numerous slick features in noisy optical remote sensing images and the current manual delineation method such as those used during the Deepwater Horizon oil spill by both academia [31] and operational agencies such as the U.S. National Oceanic and Atmospheric Administration, the proposed feature extraction method represents one step forward toward the long-term goal of fully automatic extraction.

References

[1] A. Taravat and D. F. Frate, "Development of band ratioing algorithms and neural networks to detection of oil spills using Landsat ETM+ data," *EURASIP J. Adv. Signal Process.*, vol. 107, pp. 1–8, Jan. 2012.

[2] Oil in the Sea III: Inputs, Fates, and Effects, The National Academies Press, Washington, DC, USA, 2003.

[3] M. F. Fingas and C. E. Brown, "Review of oil spill remote sensing," *Spill Sci. Technol. Bull.*, vol. 4, no. 4, pp. 199–208, 1997.

[4] C. Brekke and A. H. S. Solberg, "Oil spill detection by satellite remote sensing," *Remote Sens. Environ.*, vol. 95, no. 1, pp. 1–13, Mar. 2005.

[5] I. Leifer *et al.*, "State of the art satellite and airborne marine oil spill remote sensing: Application to the BP Deepwater Horizon oil spill," *Remote Sens. Environ.*, vol. 124, pp. 185–209, Sep. 2012.

[6] G.-P. Oscar, I. MacDonald, C. Hu, J. Svejkovsky, and M. Hess, "Detection of floating oil anomalies from the Deepwater Horizon oil spill with synthetic aperture radar," *Oceanography*, vol. 26, no. 2, pp. 124–137, 2013.

[7] C. Hu, X. Li, W. G. Pichel, and F. E. Muller-Karger, "Detection of natural oil slicks in the NW Gulf of Mexico using MODIS imagery," *Geophys. Res. Lett.*, vol. 36, pp. 1–5, Jan. 2009.

[8] G. Chust and Y. Sagarminaga, "The multi-angle view of MISR detects oil slicks under sun glitter conditions," *Remote Sens. Environ.*, vol. 107, no. 1/2, pp. 232–239, Mar. 2007.

[9] C. F. Schueler, T. F. Lee, and S. D. Miller, "VIIRS constant spatial-resolution advantages," *Int. J. Remote Sens.*, vol. 34, no. 16, pp. 5761–5777, May 2013.

[10] C. Hu, S. Chen, M. Wang, B. Murch, and J. Taylor, "Detecting surface oil slicks using VIIRS nighttime imagery under moon glint: A case study in the Gulf of Mexico," *Remote Sens. Lett.*, vol. 6, pp. 295–301, 2015.

[11] C. Han, H. Guo, C. Wang, and D. Fan, "A novel method to reduce speckle in SAR images," *Int. J. Remote Sens.*, vol. 23, no. 23, pp. 5095–5101, 2002.

[12] B. Huang, H. Li, and X. Huang, "A level set method for oil slick segmentation in SAR images," *Int. J. Remote Sens.*, vol. 26, no. 6, pp. 1145–1156, 2005.

[13] D. Espinoza Molina, D. Gleich, and M. Datcu, "Evaluation of Bayesian despeckling and texture extraction methods based on Gauss-Markov and auto-binomial Gibbs random fields: Application to TerraSAR-X data," *IEEE Trans. Geosci. Remote Sens.*, vol. 50, no. 5, pp. 2001–2025, May 2012.

[14] A. Taravat, D. Latini, and F. Del Frate, "Fully automatic dark-spot detection from SAR imagery with the combination of nonadaptive Weibull multiplicative model and pulse-coupled neural networks," *IEEE Trans. Geosci. Remote Sens.*, vol. 52, no. 5, pp. 2427–2435, May 2014.

[15] Y. Shu, J. Li, H. Yousif, and G. Gomes, "Dark-spot detection from SAR intensity imagery with spatial density thresholding for oil-spill monitoring," *Remote Sens. Environ.*, vol. 114, no. 9, pp. 2026–2035, Sep. 2010.

[16] F. Galland, P. Refregier, and O. Germain, "Synthetic aperture radar oil spill segmentation by stochastic complexity minimization," *IEEE Geosci. Remote Sens. Lett.*, vol. 1, no. 4, pp. 295–299, Oct. 2004.

[17] A. H. S. Solberg, C. Brekke, and P. Ove Husoy, "Oil spill detection in Radarsat and Envisat SAR images," *IEEE Trans. Geosci. Remote Sens.*, vol. 45, no. 3, pp. 746–755, Mar. 2007.

[18] G.-P. Oscar, B. Zimmer, M. Howard, X. L. W. Pichel, and I. R. MacDonald, "Using SAR images to delineate ocean oil slick with a Texture-Classifying Neural Network Algorithm (TCNNA)," *Can. J. Remote Sens.*, vol. 35, no. 5, pp. 411–421, 2009.

[19] K. Karantzalos and D. Argialas, "Automatic detection and tracking of oil spills in SAR imagery with level set segmentation," *Int. J. Remote Sens.*, vol. 29, no. 21, pp. 6281–6296, Nov. 2008.

[20] T. E. Lee *et al.*, "The NPOESS VIIRS day/night visible sensor," *Bull. Amer. Meteorol. Soc.*, vol. 87, no. 2, pp. 191–199, Feb. 2006.

[21] S. D. Miller, C. L. Combs, and S. Q. Kidder, "Assessing moonlight availability for nighttime environmental applications by low-light visible polar-orbiting satellite sensors," *J. Atmos. Ocean. Technol.*, vol. 29, pp. 538–557, 2011.

[22] C. R. Jackson and W. Alpers, "The role of the critical angle in brightness reversals on sunglint images of the sea surface," *J. Geophys. Res.*, vol. 115, pp. 1–15, 2010

[23] D. Fernandes, "Segmentation of SAR images with Weibull distribution," in *Proc. IGARSS*, 1998, vol. 1, pp. 24–26.

[24] Z. Otremba and J. Piskozub, "Modelling of the optical contrast of an oil film on a sea surface," *Opt. Exp.*, vol. 9, no. 8, pp. 411–416, Oct. 2001.

[25] N. Otsu, "Threshold selection method from gray-level histograms," *IEEE Trans. Syst., Man, Cybern.*, vol. SMC-9, no. 14, pp. 62–66, Jan. 1979.

[26] S. Chen and C. Hu, "In search of oil seeps in the Cariaco basin using MODIS and MERIS medium-resolution data," *Remote Sens. Lett.*, vol. 5, pp. 442–450, May 2014.

[27] X. Kang and X. Huiping, "Detection of oil spill in Mexico gulf based on MODIS data," in *Proc. ICMT*, 2010, pp. 1–4.

[28] K. A. Kvenvolden and C. K. Cooper, "Natural seepage of crude oil into the marine environment," *Geo-Marine Lett.*, vol. 23, no. 3/4, pp. 140–146, Dec. 2003.

[29] C. Wiedemann, C. Heipke, H. Mayer, and O. Jamet, "Empirical evaluation of automatically extracted road axes," in *Empirical Evaluation Techniques in Computer Vision*. Piscataway, NJ, USA: Wiley IEEE Press, 1998, pp. 172–187.

[30] C. Hu *et al.*, "Dynamic range and sensitivity requirements of satellite ocean color sensors: Learning from the past," *Appl. Opt.*, vol. 51, no. 25, pp. 6045–6062, 2012.

[31] C. Hu *et al.*, "Did the northeastern Gulf of Mexico become greener after the Deepwater Horizon oil spill?" *Geophys. Res. Lett.*, vol. 38, no. 9, May 2011, Art. ID. L09601.